Article:
Wang, X., Fan, Y., Zhang, B. et al. (2022) High discharge energy density in novel K1/2Bi1/2TiO3-BiFeO3 based relaxor ferroelectrics. Journal of the European Ceramic Society, 42 (15). pp. 7381-7387. ISSN: 0955-2219

https://doi.org/10.1016/j.jeurceramsoc.2022.08.020

Journal of the European Ceramic Society 42 (2022) 7381–7387

Contents lists available at ScienceDirect

Journal of the European Ceramic Society

journal homepage: www.elsevier.com/locate/jeurceramsoc

High discharge energy density in novel $K_{1/2}Bi_{1/2}TiO_3$-$BiFeO_3$ based relaxor ferroelectrics

Xinzhen Wang [a,b], Yongbo Fan [a], Bin Zhang [c], Ali Mostaed [d], Linhao Li [e], Antonio Feteira [f], Dawei Wang [c], Derek C. Sinclair [a], Ge Wang [a,g,*], Ian M. Reaney [a,**]

[a] Department of Materials Science and Engineering, University of Sheffield, Sheffield S1 3JD, UK
[b] School of Materials Science and Engineering, Shandong University of Science and Technology, Qingdao 266590, China
[c] Shenzhen Institute of Advanced Electronic Materials, Shenzhen Institute of Advanced Technology, Chinese Academy of Sciences, Shenzhen 518055, China
[d] Department of Materials, University of Oxford, Oxford OX1 3PH, UK
[e] School of Mathematics and Physics, Beijing University of Chemical Technology, Beijing 100013, China
[f] Materials and Engineering Research Institute, Sheffield Hallam University, Sheffield S1 1WB, UK
[g] Department of Materials, University of Manchester, Manchester S13 9PL, UK

ARTICLE INFO

Keywords:
Bismuth ferrite
Energy density
Dielectrics
Ceramic capacitors
Power electronics

ABSTRACT

An increasing number of new dielectrics are being reported for the development of next-generation ceramic capacitors for power electronics used in clean energy technologies. Here, high discharge energy density (W_{dis}) ~6.1 J cm^{-3} with efficiency (η)~72% under a pulsed field (E_{max}) of 410 kV cm^{-1} is reported along with temperature stability up to 150 °C (E_{max} = 200 kV cm^{-1}) for 0.5 $K_{0.5}Bi_{0.5}TiO_3$-0.42$BiFeO_3$-0.08$Sm(Mg_{2/3}Nb_{1/3})O_3$ (KBT-BF-SMN) bulk ceramics. The optimised composition is chemically heterogeneous but electrically homogenous, similar to several $BiFeO_3$-based dielectrics reported previously and adding to the growing body of evidence that electrical (measured at weak-field) not chemical homogeneity is the best guide to increased E_{max} and enhanced energy density. KBT-BF-SMN ceramics are therefore considered as promising candidates for pulsed power and power electronics applications.

1. Introduction

Given the importance of clean technologies and electrification in the coming decades, the development of power electronics and devices is recognised as a core future technology. Dielectric ceramic capacitors are passive components which provide superior power density due to their exceptionally fast charge-discharge rate (~μs) but are typically inferior in energy density with respect to supercapacitors and batteries [1–5] As the electric vehicle (EV) market grows, not only has the demand for batteries and supercapacitors increased but also for multilayer ceramic capacitors (MLCCs) used in electronics and subsystems [6–10]. In particular, new dielectric materials are needed to facilitate near-engine power electronics to enable ultra-fast charging solutions that facilitate durable EV performance.

Energy storage performance for dielectrics is evaluated from integration of the polarisation-electric field (P-E) loop at the maximum pulsed electric field (E_{pulse}) [1,11]. The E_{pulse} here is the maximum triangular AC electric field applied during P-E measurement. It differs from breakdown strength which is measured commercially using a continuous dc bias. The total and discharging energy density are obtained using $W_{total} = \int E_{pulse} dP$ and $W_{dis} = \int_{Pr}^{Pmax} E_{pulse} dP$, where P_{max} and P_r are maximum polarisation and remnant polarisation, respectively [1]. Thus, both large ΔP (P_{max}-P_r) and E_{pulse} are desirable for realising high W_{dis}. New electroceramics for high energy-density MLCCs need to demonstrate optimised E_{pulse} > 300 kV cm^{-1}, W_{dis} > 4 J cm^{-3}, good temperature stability of permittivity (at least 25–150 °C) as well as compatibility with low-cost internal electrodes (Ag, Ni and Ag-10%Pd) to facilitate mass market delivery.

In recent years, perovskite-type dielectrics (traditional class-II type capacitor candidates) have been reported with optimised energy storage performance based either on relaxor-ferroelectrics formed with end members that include $BaTiO_3$ (BT) [12–19], $Na_{0.5}Bi_{0.5}TiO_3$ (NBT) [20–24], $BiFeO_3$ (BF) [25–36] and antiferroelectrics such as $NaNbO_3$ (NN) [37–41] and $AgNbO_3$ (AN) [42–52]. The highest properties to date

* Corresponding author at: Department of Materials Science and Engineering, University of Sheffield, Sheffield S1 3JD, UK.
** Corresponding author.
E-mail addresses: ge.wang@manchester.ac.uk (G. Wang), i.m.reaney@sheffield.ac.uk (I.M. Reaney).

https://doi.org/10.1016/j.jeurceramsoc.2022.08.020
Received 15 July 2022; Received in revised form 29 July 2022; Accepted 8 August 2022
Available online 10 August 2022

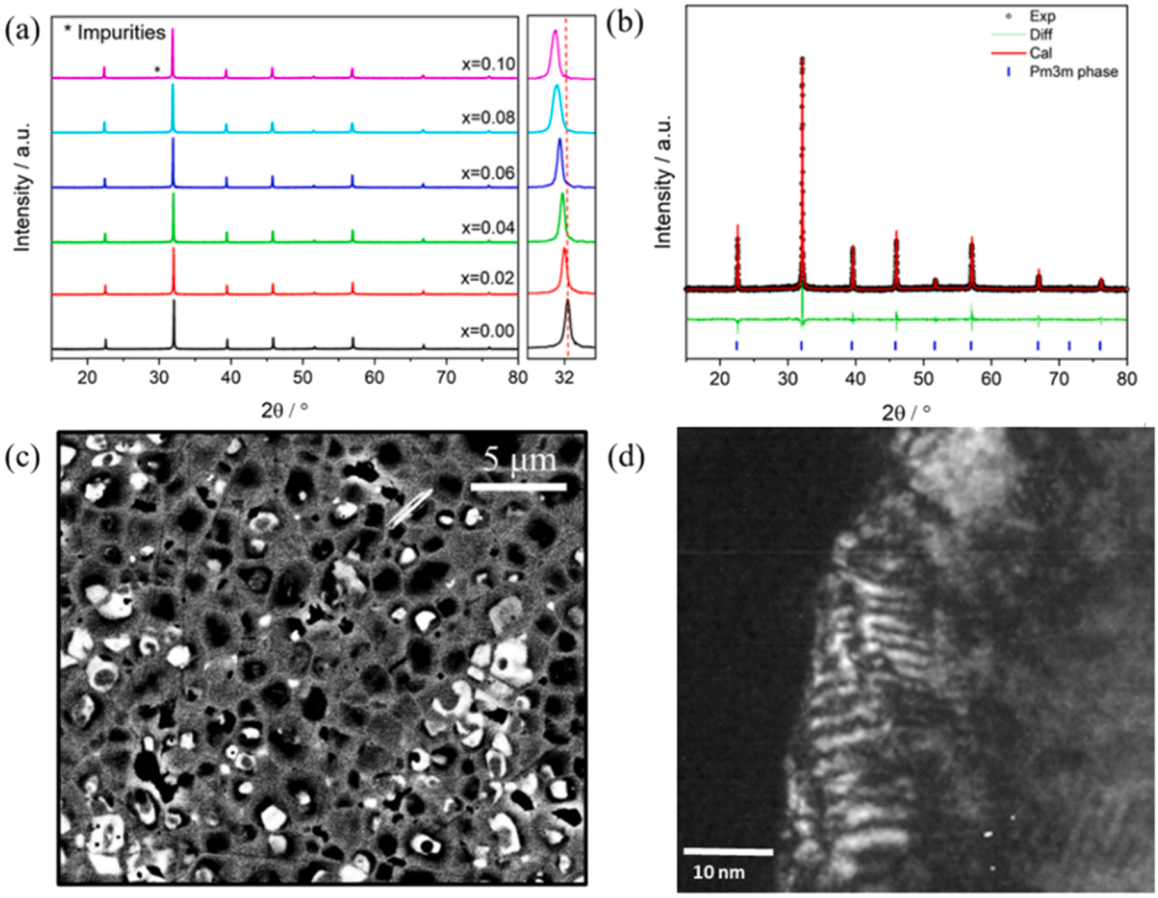

Fig. 1. (a) XRD patterns of KBT-BF-xSMN (x = 0.00–0.10) ceramics with expanded $\{110\}_p$ peaks. (b) Full-pattern Rietveld refinement using the space group $Pm\bar{3}m$ for x = 0.08. (c) BSE image of a polished ceramic surface and (d) TEM image of a grain with lamellar nanodomains for x = 0.08.

are reported for relaxor-ferroelectric compositions: W_{dis}~12.2 J cm^{-3} under E_{pulse} of 680 kVcm^{-1} was reported by Zuo *et al.* in 0.76NN-0.24NBT bulk ceramics [41] and Reaney and co-workers succeeded in tailoring the structure and electrical microstructure in BF and NBT-based systems [23,27,28,30] to give W_{dis} up to 7.5 J cm^{-3} and 18 J cm^{-3} in bulk and MLCCs, respectively. The following briefly discusses some further key findings reported for BT, AN and BF-based compositions.

Bi- and Pb-free BT compositions dominate commercial MLCCs market and are compatible with low-cost base metal electrodes but energy densities and breakdown strengths are lower than required in pulsed power and power electronic applications. Modifications using Bi based end members, e.g. $(Bi_{1/2}Li_{1/2})TaO_3$ and $Bi(Mg_{2/3}Nb_{1/3})O_3$, improve breakdown strength and energy density but necessitate the use Ag-Pd or Pt internal electrodes [12–14,18].

AN based antiferroelectrics have also been studied with a view to optimising energy density. Most studies have focused on optimising E_{pulse} and W_{dis} by stabilising the antiferroelectric with respect to the induced ferrielectric phase, thereby increasing the field required to switch to the polar rather than antipolar state [48]. To date, the highest W_{dis} for AN based bulk ceramics and MLCCs reaches approximately 7 J cm^{-3} (under E_{pulse} of 476 kV cm^{-3}) and 7.9 J cm^{-3} (under E_{pulse} of 1020 kV cm^{-1}), respectively. Most antiferroelectric type dielectrics have promising ΔP values but their energy density is restricted by reaching saturated polarisation in the induced ferroelectric phase. The associated double hysteresis loops generally show conversion efficiency, < 80%, because energy is lost through realignment of dipoles from antipolar to polar. They also suffer from large electric field-induced strain as a consequence of the field induced transition. [52] Some relaxors type dielectrics however, are reported with high E_{pulse} and energy conversion efficiency (90%). The W_{dis} also benefits from an unsaturated polarisation at higher electric field whose value increases until breakdown. Temperature stability (>200 °C) still remains a challenge for both antiferroelectric and relaxors type dielectrics.

BF based dielectrics, mostly alloyed with BT and $SrTiO_3$ (ST) demonstrate excellent performance not only as bulk ceramics (W_{dis} up to 7.5 J cm^{-3}) but also as MLCCs (W_{dis} up to 15 J cm^{-3}) and thin films (W_{dis} up to 150 J cm^{-3}) [27,28,53]. Their conduction mechanisms (p- or n-type) and electrical microstructures (electrical homogeneity) that underpin superior E_{pulse} were investigated by Wang, Reaney and co-workers who proposed several key factors to enhance the energy storage performance [27,28], such as: reduction in conductivity (controlling defect chemistry); a homogeneous electrical microstructure and a reduction in polar coupling whilst retaining ions with high average ionic polarisability. Several workers have also noted "core-shell" microstructures (bulk ceramics and MLCCs), particularly in BF-BT, but it remains to be elucidated whether these are critical to enhancing energy density [23,27,28,53].

Despite promising energy densities in many current ceramic systems, most experience a widening of the P-E loops at > 100 °C associated with the onset of the movement of V_O under applied field [30]. In 2013, BF-$K_{0.5}Bi_{0.5}TiO_3$ (BF-KBT) based ceramics were reported as high-temperature, piezoelectrics and multiferroics [54–57] with for example, BF-KBT-$PbTiO_3$ exhibiting good piezoelectric properties up to 450 °C [54]. Temperature stable and fatigue-resistant ceramics, KBT-BF-$NdFeO_3$ were also reported by Khesro *et al.* to exhibit strain variation < 10% up to 175 °C for bulk ceramics and < 15% for MLCCs up to 300 °C [58]. However, KBT is difficult to densify via conventional

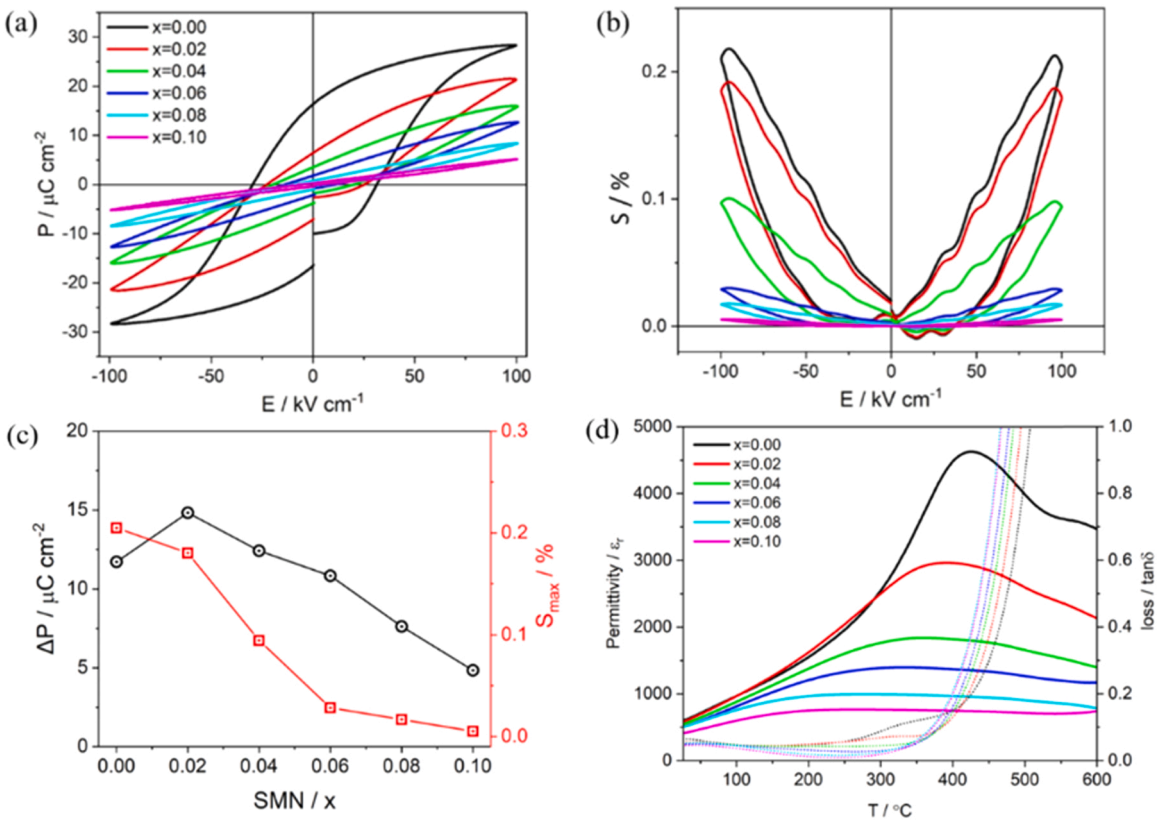

Fig. 2. (a) Bipolar P-E loops and (b) bipolar S-E loops for KBT-BF-xSMN ceramics (x = 0.00–0.10). (c) The changes of ΔP and S_{max} versus SMN concentration, x. (d) Temperature-dependent permittivity and dielectric loss data for KBT-BF-xSMN (x = 0.00–0.10) ceramics at 100 kHz.

solid-state reaction due to volatilisation of K. Therefore, few studies have investigated KBT based compositions as potential candidates for high energy density capacitors with hot pressing often employed to densify ceramics and only modest energy storage properties reported. [59–64].

Here, we report an electrically homogenous, highly-resistive relaxor, 0.5 $K_{0.5}Bi_{0.5}TiO_3$-0.42$BiFeO_3$-0.08$Sm(Mg_{2/3}Nb_{1/3})O_3$ (KBT-BF-0.08SMN), prepared using conventional solid-state synthesis that exhibits low dielectric loss (tanδ <0.04% up to 375 °C), excellent energy storage performance (W_{rec} ~ 6.1 J cm^{-3} at E_{pulse} ~ 410 kV cm^{-1}) and < 15% change in W_{dis} up to 150 °C at E_{max} ~200 kV cm^{-1}.

2. Experimental procedure

0.5KBT-(0.5-x)BF-xSMN (x = 0.00–0.10) ceramics were prepared via conventional solid-state reaction using Bi_2O_3 (>99.9%, Sigma Aldrich), Fe_2O_3 (>99%, Sigma Aldrich), K_2CO_3 (>99%, Sigma Aldrich), TiO_2 (>99.9%, Sigma Aldrich), Sm_2O_3 (>99.9%, Sigma Aldrich), MgO (>99.9%, Sigma Aldrich) and Nb_2O_5 (>99.5%, Sigma Aldrich). All reagents were weighed, ball milled for 8 h in isopropanol and calcined for 2 h at 850 °C. Calcined powders were then ball-milled again for 8 h and the dried powders uniaxially pressed into 10 mm diameter pellets. The pressed pellets were sintered at 1050–1110 °C for 2 h in air. The densities of the sintered pellets were measured using the Archimedes method.

Ceramic pellets were crushed into powder and annealed 4 h at 650 °C to remove any strain induced artefacts prior to performing X-ray diffraction. The phase purity and crystal structures of the ceramics were examined using a Bruker D2 phaser X-ray powder diffractometer (XRD) with a CuKα radiation (λ = 0.15406 nm). Full-pattern Rietveld refinement was performed using TOPAS 5 to obtain crystallographic information. The specimens were ground using 1200, 2500, 4000-grade SiC paper, followed by a polishing using 6, 3 and 1 μm diamond pastes. Ceramic microstructures were studied using an FEI Inspect F50 scanning electron microscope equipped with back scattered electron (BSE) and energy dispersive X-ray spectroscopy (EDX) detectors. Powders of selected ceramics were analysed by high-resolution transmission electron microscopy (HRTEM) using a JEOL 2100.

Ceramic pellets were lightly ground and fired with gold electrode at 850 °C for 2 h prior to electrical measurements. Temperature-dependent dielectric properties were studied using an Agilent 4184 A precision LCR meter from room temperature (RT) to 600 °C at 10, 100, 250 kHz and 1 MHz. Impedance spectroscopy was performed using an Agilent E4980A impedance AC analyser from room temperature to 400 °C. Impedance data were normalised by a geometric factor (thickness/surface) and estimated resistivity was obtained using ZView software. Specimens for unipolar polarisation-field (P-E) and strain-field (S-E) measurements were ground to 0.2 mm and sputtered with Au electrodes using an Agar sputter coater. Unipolar P-E and S-E loops were obtained a using AixACCT TF Analyzer 2000 ferroelectric tester at 1 Hz from room temperature to 150 °C.

3. Results and discussion

XRD patterns of powders from the KBT-BF-xSMN ceramics (x = 0.00–0.10) are shown in Fig. 1a. All samples with x < 0.10 could be indexed according to a single perovskite phase whereas a non-perovskite secondary phase was detected by XRD for x = 0.10. Full-pattern Rietveld refinements were performed using cubic ($Pm\bar{3}m$), rhombohedral ($R3c$) and tetragonal ($P4mm$) space groups. The best refinement results (GOF=1.05–1.15) for all compositions were obtained based on a cubic $Pm\bar{3}m$ phase, Fig. 1b and Table S1 (SI). BSE images of polished KBT-BF-xSMN surfaces are shown in Fig. 1c and Fig. S1(SI). A complex "core-shell" microstructure was observed for all compositions, with some

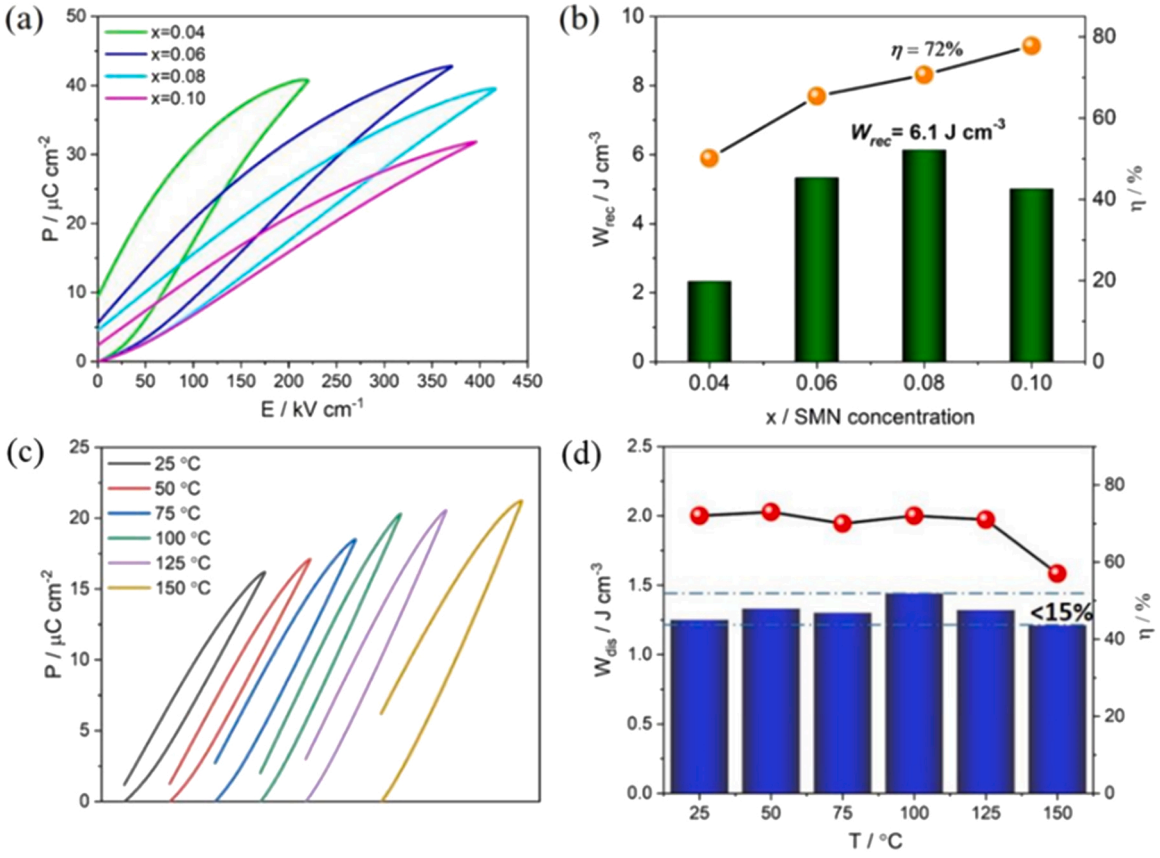

Fig. 3. (a) Unipolar P-E loops at E_{max} and (b) W_{dis} and η values for KBT-BF-xSMN (x = 0.04–0.10) ceramics. (c) Temperature-dependent unipolar P-E loops and (d) calculated W_{dis} and η for x = 0.08 ceramics.

exhibiting dark Bi-deficient and others bright Bi-rich cores (Fig. S2 SI). This unique microstructural behaviour is formed due to kinetic limitation of the diffusion process and immiscibility on cooling from high temperature. It is reminiscent of that observed by Wang and co-workers [27] in their BF-BT based compositions which despite their chemical inhomogeneity were electrically homogeneous. It has also been reported in other lead-free perovskites, such as $NaNbO_3$ and BT based bulk ceramics [65,66]. An additional grain boundary (bright) phase was also present for x = 0.10, presumably corresponding to the impurity secondary peaks in XRD patterns (Fig. 1a). Unlike in BF based ceramics, the average grain size of the KBT-BF-xSMN solid solutions remained broadly the same irrespective of the value of x, 2.95 ± 0.56 μm for x = 0.00 and 2.14 ± 0.28 μm for x = 0.08, Table S2 (SI). The local microstructure of x = 0.08 was further examined by TEM with lamellar-like nano-domains (~10 nm) observed within grains, Fig. 1d. Although longer in length than the nano-regions expected for true relaxor ferroelectrics, the lamellar domains indicate a reduced coherence length of polarisation compared with KBT [67].

Bipolar P-E loops at 100 kV cm^{-1} for KBT-BF-xSMN (x = 0.00–0.10) ceramics are shown in Fig. 2a. The highest P_{max}~29 μC cm^{-2} and P_r~17 μC cm^{-2} are for x = 0.00 with both decreasing with increasing x. The highest ΔP~15 μC cm^{-2} was obtained for x = 0.02, followed by a gradual decrease with increasing x, Fig. 2c. Bipolar S-E loops at 100 kV cm^{-1} for KBT-BF-SMN (x = 0.00–0.10) ceramics are displayed in Fig. 2b. Electrostrictive-like S-E behaviour is dominant for compositions with x > 0.00, suggesting compositions on the whole have a relaxor-like response. We note however, that some negative strain is observed for x = 0, consistent with the appearance of a ferroelectric hysteresis loop. x = 0.00 showed the highest electric field-induced strain of ~0.22% which decreased with increasing x. For x > 0.04, essentially linear P-E loops (P_r close to zero) and negligible electric field-induced strain (S_{max}<0.05%) were obtained (Figs. 2b and 2c), both of which are desirable for energy storage performance and reliability. The temperature-dependent dielectric permittivity (ε_r vs. T) and dielectric loss (tan δ vs. T) data at 100 kHz for KBT-BF-xSMN (x = 0.00–0.10) ceramics are shown in Fig. 2d. A frequency-dependent broad peak in ε_r at ~410 °C (100 kHz data) (Fig. S3 SI) was observed for x = 0.00, confirming relaxor-behaviour. As x increases, the ε_r vs. T plots become flatter with ε_r(max) decreasing from ~5500–900, the latter varying by < ±15% between 130 and 600 °C. For tan δ vs. T, tan δ (<0.05) remains low from RT to ~ 350 °C for all compositions, followed by a sharp rise above 400 °C.

The unipolar P-E loops up to maximum E_{pulse} and the calculated energy storage performance for x = 0.04–0.10 are shown in Fig. S4 and S5 (SI). For x = 0.00 and 0.02, energy storage performance was not evaluated due to low E_{pulse} and η. The maximum E_{pulse} for the three single phase compositions above x = 0.02 increases with increasing x, with the highest E_{pulse}= 410 kV cm^{-1} obtained for x = 0.08, as shown in Fig. 3a. The P-E loops become slimmer with increasing x, resulting in the highest W_{dis}~6.1 J cm^{-3} and η~72% for x = 0.08 at 410 kV cm^{-1}. The highest η~82% was obtained for x = 0.10, as shown in Fig. 3b, yielding W_{dis}= 5.2 J cm^{-3} at 400 kV cm^{-1}. The temperature-dependent unipolar P-E behaviour at 200 kV cm^{-1} for x = 0.08 was also evaluated to investigate temperature stability of the bulk ceramics, Fig. 3c. W_{dis} (Fig. 3d) exhibits relatively good temperature stability (<15% variation at 200 kV cm^{-1}) from ~ 25–150 °C, which is important for practical applications during operation. The widening of the P-E loop > 150 °C here has been found in other BF based system [27,28] and is generally attributed to either the diffusion oxygen vacancies or an electric field-induced phase transition. In previous studies the latter has been postulated as more likely due to the inherently low strain [27,28].

As reported for previous BF-based compositions, electrical

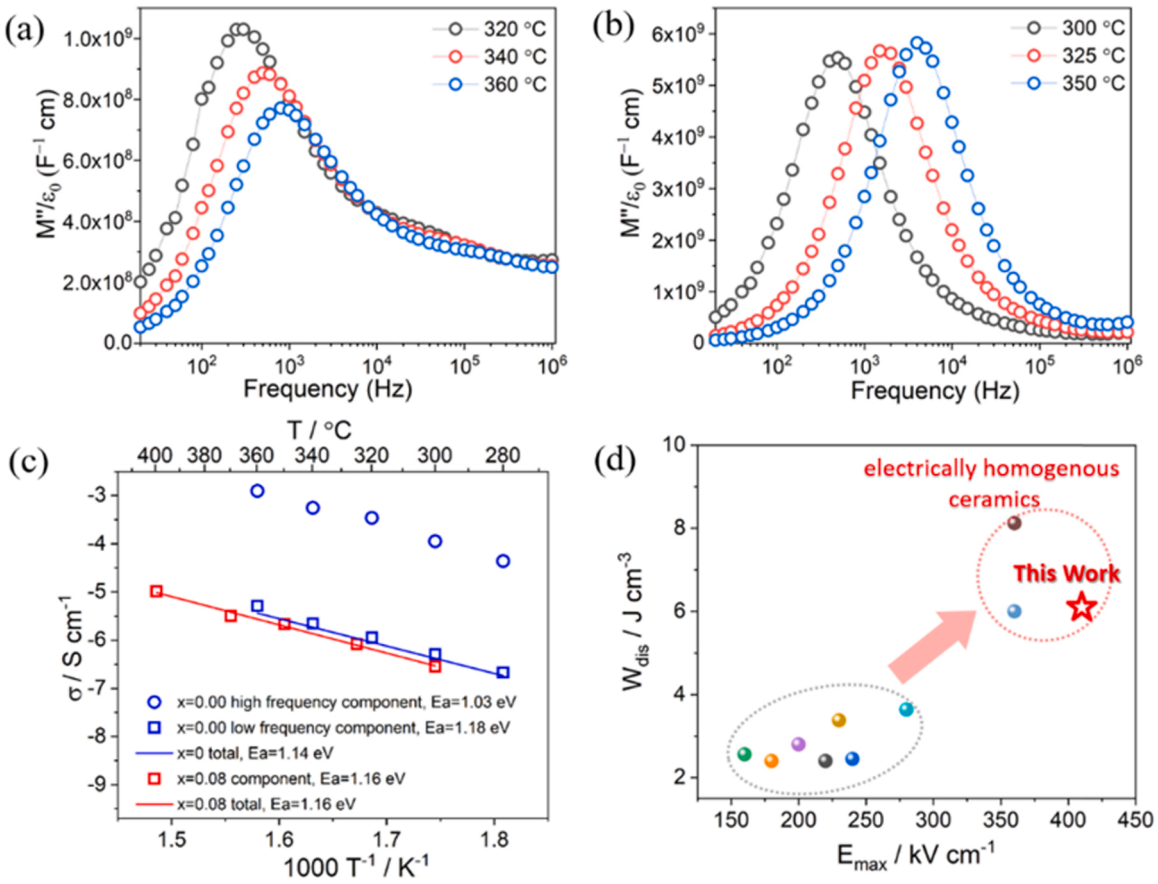

Fig. 4. Temperature-dependent M'' spectroscopic plots for (a) x = 0.00 and (b) x = 0.08. (c) Arrhenius plots for x = 0.00 and x = 0.08. (d) Comparison of W_{dis} and E_{max} for BF-containing ceramics reported in the literature [25,27–32,34].

homogeneity plays an important role in optimising energy density.[27] The electrical microstructure of KBT-BF (x = 0.00) and KBT-BF-0.08SMN (x = 0.08) ceramics were examined using impedance spectroscopy. M'' spectroscopic plot of x = 0.00 exhibit one main M'' peak at lower frequency (lower-*f*) of 10^2-10^3 Hz and a second small peak at the higher frequency (higher-*f*) of 10^4-10^5 Hz (Fig. 4a), indicating an inhomogeneous electrical microstructure. At 360 °C, the corresponding capacitance values of the two M'' peaks are 6.47×10^{-10} and 1.65×10^{-9} F cm^{-1}, respectively, and are interpreted as bulk components [68]. The resistivity of the lower-*f* and higher-*f* components are estimated to be 307.7 and 0.8 kΩ using the relationship ωRC= 1. In contrast, a single peak is observed in the M'' spectroscopic plot at 350 °C, corresponding to single bulk component with C~8.58×10^{-11} F cm^{-1} and resistivity of 463.7 kΩ, indicating an electrical homogeneous microstructure (Fig. 4b).

The total resistivities of x = 0.00 and x = 0.08, obtained from the intercept of the arc from Z * plots, were 91 and 97 kΩ cm at 400 °C (Fig. S6 SI), respectively. The total activation energies, obtained from the intercept of complex Z * plots, were similar for x = 0.00 (E_a=1.14 eV) and x = 0.08 (E_a=1.16 eV), Fig. 4c, which is also comparable to other reported compositions, such as BF-BT and BF-ST based ceramics (1.14–1.18 eV) [28,30,69]. It is worth noting that the conductivity for low-*f* component (resistive shell) of x = 0.00 is approximately level up with the total conductivity for x = 0.08. However, the higher-*f* component (conductive core) of x = 0.00 is more conductive (at least two order of magnitude) with lower E_a= 1.03 eV compared to the lower-*f* bulk conductivity, leading to potential early breakdown at lower electric field. In contrast, the higher E_a~1.16 eV coupled with the electrical homogeneity of x = 0.08 favour increasing E_{pulse}. Both compositions are observed to exhibit core-shell microstructure but perhaps the difference on conductivity between conductive higher-*f* component (BF-rich core) and resistive lower-*f* component (KBT-rich shell) is significate for x = 0.00. While Nb^{5+} from SMN doping could possible suppress the conductivity in BF-rich conductive core, allowing electrical microstructure to be homogeneous for x = 0.08. The electrical homogeneity demonstrated above suggests that the fabrication of MLCC prototypes with high E_{max} is feasible due to the absence of conductive pathways. Although it may seem counterintuitive that compositions with chemical inhomogeneity are electrically homogeneous, these observation are consistent with other BF-based ceramics [25,27–32,34,35] that have been used to form high E_{pulse} (1 MV cm^{-1}) prototype MLCCs. Apart from BF-based ceramics, achieving electrical homogeneity also enhances W_{dis} in other lead-free systems, such as BT- [70] and NBT-based [23,71] bulk ceramics.

4. Conclusions

KBT-BF-xSMN (x = 0.00–0.10) ceramics were successfully synthesised by solid-state reaction. All compositions had an average (pseudo) cubic structure (XRD), albeit with evidence of lamellar ferroelectric nanodomains by TEM, and exhibited a complex, chemically inhomogeneous "core-shell" microstructure (SEM). However, the electrical microstructure of x = 0.08 was homogeneous with an E_a value of 1.18 eV, allowing the composition to achieve excellent energy storage performance, W_{dis}= 6.1 J cm^{-3} and η = 72%, under E_{pulse} ~410 kV cm^{-1}. In addition, to the high discharging density, KBT-BF-xSMN show a temperature stable ε_r from 130 to 600 °C with very little frequency dependence from 10 kHz to 1 MHz and retain their pulsed discharge characteristics until 150 °C at 200 kVcm^{-1}. This material is therefore a potential candidate for next-generation energy-density

prototype MLCCs, provided a low-cost internal electrode system can be found.

Declaration of Competing Interest

The authors declare that they have no known competing financial interests or personal relationships that could have appeared to influence the work reported in this paper.

Acknowledgements

We thank the Engineering and Physical Science Research Council for funding FPeT: Framework for designing piezoelectric transformer power supplies (EP/P015859/1) and Leverhulme Trust their support of 'Understanding the mixing and properties of high entropy perovskites'. We also thank support provided by Functional Materials and Devices group from The University of Sheffield.

Appendix A. Supporting information

Supplementary data associated with this article can be found in the online version at doi:10.1016/j.jeurceramsoc.2022.08.020.

References

[1] G. Wang, Z. Lu, Y. Li, L. Li, H. Ji, A. Feteira, D. Zhou, D. Wang, S. Zhang, I. M. Reaney, Electroceramics for high-energy density capacitors: current status and future perspectives, Chem. Rev. 121 (10) (2021) 6124–6172.
[2] Y. Sakabe, Multilayer ceramic capacitors, Curr. Opin. Solid State Mater. Sci. 2 (5) (1997) 584–587.
[3] N.H. Fletcher, A.D. Hilton, B.W. Ricketts, Optimization of energy storage density in ceramic capacitors, J. Phys. D Appl. Phys. 29 (1) (1996) 253–258.
[4] G.R. Love, Energy storage in ceramic dielectrics, J. Am. Ceram. Soc. 73 (2) (1990) 323–328.
[5] I. Burn, D.M. Smyth, Energy storage in ceramic dielectrics, J. Mater. Sci. 7 (3) (1972) 339–343.
[6] Multilayer Ceramic Capacitor Market, Global Opportunity Analysis and Industry Forecast, 2018–2024, Allied Market Research SE_184655 (2018).
[7] R.U. Masao Yano, History of power electronics in Japan, IEEJ Trans. Fundam. Mater. 121 (1) (2001) 2–10.
[8] S. Siami, C. Joubert, C. Glaize, High frequency model for power electronics capacitors, IEEE Trans. Power Electron 16 (2) (2001) 157–166.
[9] M.S. Whittingham, Materials challenges facing electrical energy storage, MRS Bull. 33 (4) (2008) 411–419.
[10] M. Yano, S. Abe, E. Ohno, History of power electronics for motor drives in Japan, IEEE Conf. Hist. Electron. (2004) 1–11.
[11] J. Wang, Z.-H. Shen, Modeling-guided understanding microstructure effects in energy storage dielectrics, Microstructures 1 (1) (2021) 2021006.
[12] W.-B. Li, D. Zhou, L.-X. Pang, R. Xu, H.-H. Guo, Novel barium titanate based capacitors with high energy density and fast discharge performance, J. Mater. Chem. A 5 (37) (2017) 19607–19612.
[13] W.-B. Li, D. Zhou, R. Xu, L.-X. Pang, I.M. Reaney, $BaTiO_3$–$Bi(Li_{0.5}Ta_{0.5})O_3$, lead-free ceramics, and multilayers with high energy storage density and efficiency, ACS Appl. Energy Mater. 1 (9) (2018) 5016–5023.
[14] W.-B. Li, D. Zhou, R. Xu, D.-W. Wang, J.-Z. Su, L.-X. Pang, W.-F. Liu, G.-H. Chen, $BaTiO_3$-based multilayers with outstanding energy storage performance for high temperature capacitor applications, ACS Appl. Energy Mater. 2 (8) (2019) 5499–5506.
[15] H. Wang, P. Zhao, L. Chen, L. Li, X. Wang, Energy storage properties of $0.87BaTiO_3$-$0.13Bi(Zn_{2/3}(Nb_{0.85}Ta_{0.15})_{1/3})O_3$ multilayer ceramic capacitors with thin dielectric layers, J. Adv. Ceram. 9 (3) (2020) 292–302.
[16] H. Wang, P. Zhao, L. Chen, X. Wang, Effects of dielectric thickness on energy storage properties of $0.87BaTiO_3$-$0.13Bi(Zn_{2/3}(Nb_{0.85}Ta_{0.15})_{1/3})O_3$ multilayer ceramic capacitors, J. Eur. Ceram. Soc. 40 (5) (2020) 1902–1908.
[17] H. Yang, Z. Lu, L. Li, W. Bao, H. Ji, J. Li, A. Feteira, F. Xu, Y. Zhang, H. Sun, Z. Huang, W. Lou, K. Song, S. Sun, G. Wang, D. Wang, I.M. Reaney, Novel $BaTiO_3$-based, Ag/Pd-compatible lead-free relaxors with superior energy storage performance, ACS Appl. Mater. Interfaces 12 (39) (2020) 43942–43949.
[18] W.-B. Li, D. Zhou, W.-F. Liu, J.-Z. Su, F. Hussain, D.-W. Wang, G. Wang, Z.-L. Lu, Q.-P. Wang, High-temperature $BaTiO_3$-based ternary dielectric multilayers for energy storage applications with high efficiency, Chem. Eng. J. 414 (2021), 128760.
[19] H. Yang, W. Bao, Z. Lu, L. Li, H. Ji, Y. Huang, F. Xu, G. Wang, D. Wang, High-energy storage performance in $BaTiO_3$-based lead-free multilayer ceramic capacitors, J. Mater. Res. 36 (6) (2021) 1285–1294.
[20] N. Truong-Tho, L.D. Vuong, Effect of sintering temperature on the dielectric, ferroelectric and energy storage properties of SnO_2-doped $Bi_{0.5}(Na_{0.8}K_{0.2})_{0.5}TiO_3$ lead-free ceramics, J. Adv. Dielectr. 10 (04) (2020) 2050011.
[21] S. Uddin, G.-P. Zheng, A. Khan, M.R. Khan, B. Khan, Temperature-dependent energy storage characterization of Pb-free relaxor ferroelectrics, J. Adv. Dielectr. 10 (03) (2020) 2050009.
[22] A. Manan, M.U. Rehman, A. Ullah, A.S. Ahmad, Y. Iqbal, I. Qazi, M.A. Khan, H. U. Shah, A.H. Wazir, High energy storage density with ultra-high efficiency and fast charging–discharging capability of sodium bismuth niobate lead-free ceramics, J. Adv. Dielectr. 11 (04) (2021) 2150018.
[23] H. Ji, W. Bao, Z. Lu, G. Wang, J. Li, H. Yang, A. Mostaed, L. Li, A. Feteira, F. Xu, D.-j Li, G. Liu, D. Wang, S.-Y. Liu, I.M. Reaney, Ultrahigh energy density in short-range tilted lead-free multilayer ceramic capacitors by nanodomain percolation, Energy Storage Mater. 38 (2021) 113–120.
[24] S. Zhou, Y. Pu, X. Zhao, T. Ouyang, J. Ji, Q. Zhang, C. Zhang, S. Sun, R. Sun, J. Li, D. Wang, Dielectric temperature stability and energy storage performance of NBT-based ceramics by introducing high-entropy oxide, J. Am. Ceram. Soc. 105 (7) (2022) 4796–4804.
[25] D. Wang, Z. Fan, W. Li, D. Zhou, A. Feteira, G. Wang, S. Murakami, S. Sun, Q. Zhao, X. Tan, I.M. Reaney, High energy storage density and large strain in $Bi(Zn_{2/3}Nb_{1/3})O_3$-doped $BiFeO_3$–$BaTiO_3$ ceramics, ACS Appl. Energy Mater. 1 (8) (2018) 4403–4412.
[26] D. Wang, Z. Fan, D. Zhou, A. Khesro, S. Murakami, A. Feteira, Q. Zhao, X. Tan, Ian M. Reaney, Bismuth ferrite-based lead-free ceramics and multilayers with high recoverable energy density, J. Mater. Chem. A 6 (9) (2018) 4133–4144.
[27] G. Wang, J. Li, X. Zhang, Z. Fan, F. Yang, A. Feteira, D. Zhou, D.C. Sinclair, T. Ma, X. Tan, D. Wang, I.M. Reaney, Ultrahigh energy storage density lead-free multilayers by controlled electrical homogeneity, Energy Environ. Sci. 12 (2) (2019) 582–588.
[28] Z. Lu, G. Wang, W. Bao, J. Li, L. Li, A. Mostaed, H. Yang, H. Ji, D. Li, A. Feteira, F. Xu, D. Sinclair, D. Wang, S.-Y. Liu, I. Reaney, Superior energy density through tailored dopant strategies in multilayer ceramic capacitors, Energy Environ. Sci. 13 (2020) 2938–2948.
[29] G. Wang, Z. Lu, J. Li, H. Ji, H. Yang, L. Li, S. Sun, A. Feteira, H. Yang, R. Zuo, D. Wang, I.M. Reaney, Lead-free $(Ba,Sr)TiO_3$–$BiFeO_3$ based multilayer ceramic capacitors with high energy density, J. Eur. Ceram. Soc. 40 (4) (2020) 1779–1783.
[30] G. Wang, Z. Lu, H. Yang, H. Ji, A. Mostaed, L. Li, Y. Wei, A. Feteira, S. Sun, D. C. Sinclair, D. Wang, I.M. Reaney, Fatigue resistant lead-free multilayer ceramic capacitors with ultrahigh energy density, J. Mater. Chem. A 8 (22) (2020) 11414–11423.
[31] Z. Chen, X. Bu, B. Ruan, J. Du, P. Zheng, L. Li, F. Wen, W. Bai, W. Wu, L. Zheng, Y. Zhang, Simultaneously achieving high energy storage density and efficiency under low electric field in $BiFeO_3$-based lead-free relaxor ferroelectric ceramics, J. Eur. Ceram. Soc. 40 (15) (2020) 5450–5457.
[32] N. Liu, R. Liang, Z. Zhou, X. Dong, Designing lead-free bismuth ferrite-based ceramics learning from relaxor ferroelectric behavior for simultaneous high energy density and efficiency under low electric field, J. Mater. Chem. C 6 (38) (2018) 10211–10217.
[33] Z. Chen, X. Bai, H. Wang, J. Du, W. Bai, L. Li, F. Wen, P. Zheng, W. Wu, L. Zheng, Y. Zhang, Achieving high-energy storage performance in $0.67Bi_{1-x}Sm_xFeO_3$-$0.33BaTiO_3$ lead-free relaxor ferroelectric ceramics, Ceram. Int. 46 (8, Part B) (2020) 11549–11555.
[34] H. Yang, H. Qi, R. Zuo, Enhanced breakdown strength and energy storage density in a new $BiFeO_3$-based ternary lead-free relaxor ferroelectric ceramic, J. Eur. Ceram. Soc. 39 (8) (2019) 2673–2679.
[35] H. Qi, A. Xie, A. Tian, R. Zuo, Superior energy-storage capacitors with simultaneously giant energy density and efficiency using nanodomain engineered $BiFeO_3$-$BaTiO_3$-$NaNbO_3$ lead-free bulk ferroelectrics, Adv. Energy Mater. 10 (6) (2020) 1903338.
[36] F. Yan, H. Bai, G. Ge, J. Lin, C. Shi, K. Zhu, B. Shen, J. Zhai, S. Zhang, Composition and structure optimized $BiFeO_3$-$SrTiO_3$ lead-free ceramics with ultrahigh energy storage performance, Small 18 (10) (2022) 2106515.
[37] H. Chen, J. Shi, X. Chen, C. Sun, F. Pang, X. Dong, H. Zhang, H. Zhou, Excellent energy storage properties and stability of $NaNbO_3$–$Bi(Mg_{0.5}Ta_{0.5})O_3$ ceramics by introducing $(Bi_{0.5}Na_{0.5})_{0.7}Sr_{0.3}TiO_3$, J. Mater. Chem. A (2021).
[38] X. Dong, X. Li, X. Chen, H. Chen, C. Sun, J. Shi, F. Pang, H. Zhou, High energy storage density and power density achieved simultaneously in $NaNbO_3$-based lead-free ceramics via antiferroelectricity enhancement, J. Mater. 7 (3) (2021) 629–639.
[39] C. Sun, X. Chen, J. Shi, F. Pang, X. Dong, Hy Chen, K. Wang, X. Zhou, H. Zhou, Simultaneously with large energy density and high efficiency achieved in $NaNbO_3$-based relaxor ferroelectric ceramics, J. Eur. Ceram. Soc. 41 (3) (2021) 1891–1903.
[40] H. Qi, R. Zuo, Linear-like lead-free relaxor antiferroelectric $(Bi_{0.5}Na_{0.5})TiO_3$–$NaNbO_3$ with giant energy-storage density/efficiency and super stability against temperature and frequency, J. Mater. Chem. A 7 (8) (2019) 3971–3978.
[41] H. Qi, R. Zuo, A. Xie, A. Tian, J. Fu, Y. Zhang, S. Zhang, Ultrahigh energy-storage density in $NaNbO_3$-based lead-free relaxor antiferroelectric ceramics with nanoscale domains, Adv. Funct. Mater. 29 (35) (2019) 1903877.
[42] Y. Tian, L. Jin, H. Zhang, Z. Xu, X. Wei, E.D. Politova, S.Y. Stefanovich, N. V. Tarakina, I. Abrahams, H. Yan, High energy density in silver niobate ceramics, J. Mater. Chem. A 4 (44) (2016) 17279–17287.
[43] Y. Tian, L. Jin, H. Zhang, Z. Xu, X. Wei, G. Viola, I. Abrahams, H. Yan, Phase transitions in bismuth-modified silver niobate ceramics for high power energy storage, J. Mater. Chem. A 5 (33) (2017) 17525–17531.
[44] J. Gao, Y. Zhang, L. Zhao, K.-Y. Lee, Q. Liu, A. Studer, M. Hinterstein, S. Zhang, J. Li, Enhanced antiferroelectric phase stability in La-doped $AgNbO_3$: Perspectives from the microstructure to energy storage properties, J. Mater. Chem. A 7 (2018) 2225–2232.
[45] K. Han, N. Luo, S. Mao, F. Zhuo, L. Liu, B. Peng, X. Chen, C. Hu, H. Zhou, Y. Wei, Ultrahigh energy-storage density in A-/B-site co-doped $AgNbO_3$ lead-free

antiferroelectric ceramics: insight into the origin of antiferroelectricity, J. Mater. Chem. A 7 (46) (2019) 26293–26301.
[46] N. Luo, K. Han, F. Zhuo, C. Xu, G. Zhang, L. Liu, X. Chen, C. Hu, H. Zhou, Y. Wei, Aliovalent A-site engineered $AgNbO_3$ lead-free antiferroelectric ceramics toward superior energy storage density, J. Mater. Chem. A 7 (23) (2019) 14118–14128.
[47] Y. Tian, L. Jin, Q. Hu, K. Yu, Y. Zhuang, G. Viola, I. Abrahams, Z. Xu, X. Wei, H. Yan, Phase transitions in tantalum-modified silver niobate ceramics for high power energy storage, J. Mater. Chem. A 7 (2) (2019) 834–842.
[48] Z. Lu, W. Bao, G. Wang, S.-k Sun, L. Li, J. Li, H. Yang, H. Ji, A. Feteira, D. Li, F. Xu, A.K. Kleppe, D. Wang, S.-Y. Liu, I.M. Reaney, Mechanism of enhanced energy storage density in $AgNbO_3$-based lead-free antiferroelectrics, Nano Energy 79 (2020), 105423.
[49] N. Luo, K. Han, M.J. Cabral, X. Liao, S. Zhang, C. Liao, G. Zhang, X. Chen, Q. Feng, J.-F. Li, Y. Wei, Constructing phase boundary in $AgNbO_3$ antiferroelectrics: pathway simultaneously achieving high energy density and efficiency, Nat. Commun. 11 (1) (2020) 4824.
[50] D. Yang, J. Gao, L. Shu, Y.-X. Liu, J. Yu, Y. Zhang, X. Wang, B.-P. Zhang, J.-F. Li, Lead-free antiferroelectric niobates $AgNbO_3$ and $NaNbO_3$ for energy storage applications, J. Mater. Chem. A 8 (2020) 23724–23737.
[51] S. Li, T. Hu, H. Nie, Z. Fu, C. Xu, F. Xu, G. Wang, X. Dong, Giant energy density and high efficiency achieved in silver niobate-based lead-free antiferroelectric ceramic capacitors via domain engineering, Energy Storage Mater. 34 (2021) 417–426.
[52] L.-F. Zhu, L. Zhao, Y. Yan, H. Leng, X. Li, L.-Q. Cheng, X. Xiong, S. Priya, Composition and strain engineered $AgNbO_3$-based multilayer capacitors for ultra-high energy storage capacity, J. Mater. Chem. A 9 (15) (2021) 9655–9664.
[53] H. Pan, F. Li, Y. Liu, Q. Zhang, M. Wang, S. Lan, Y. Zheng, J. Ma, L. Gu, Y. Shen, P. Yu, S. Zhang, L.-Q. Chen, Y.-H. Lin, C.-W. Nan, Ultrahigh–energy density lead-free dielectric films via polymorphic nanodomain design, Science 365 (6453) (2019) 578.
[54] J. Bennett, A.J. Bell, T.J. Stevenson, T.P. Comyn, Tailoring the structure and piezoelectric properties of $BiFeO_3$-$(K_{0.5}Bi_{0.5})TiO_3$-$PbTiO_3$ ceramics for high temperature applications, Appl. Phys. Lett. 103 (15) (2013), 152901.
[55] Y. Li, Z. Zhang, Y. Chen, D.A. Hall, Electric field-induced strain in core-shell structured $BiFeO_3K_{0.5}Bi_{0.5}TiO_3PbTiO_3$ ceramics, Acta Mater. 160 (2018) 199–210.
[56] Y. Li, Y. Chen, Z. Zhang, A. Kleppe, D.A. Hall, In-situ XRD study of actuation mechanisms in $BiFeO_3$-$K_{0.5}Bi_{0.5}TiO_3$-$PbTiO_3$ ceramics, Acta Mater. 168 (2019) 411–425.
[57] Y. Li, P.I. Cowin, B. Wang, A. Kleppe, T.P. Comyn, D.A. Hall, Actuation mechanisms in mixed-phase $K_{0.5}Bi_{0.5}TiO_3$-$BiFeO_3$-$PbTiO_3$ ceramics, J. Eur. Ceram. Soc. 41 (13) (2021) 6414–6423.
[58] A. Khesro, D. Wang, F. Hussain, D.C. Sinclair, A. Feteira, I.M. Reaney, Temperature stable and fatigue resistant lead-free ceramics for actuators, Appl. Phys. Lett. 109 (14) (2016), 142907.
[59] F. Li, T. Jiang, J. Zhai, B. Shen, H. Zeng, Exploring novel bismuth-based materials for energy storage applications, J. Mater. Chem. C 6 (30) (2018) 7976–7981.
[60] F. Li, X. Hou, T. Li, R. Si, C. Wang, J. Zhai, Fine-grain induced outstanding energy storage performance in novel $Bi_{0.5}K_{0.5}TiO_3$-$Ba(Mg_{1/3}Nb_{2/3})O_3$ ceramics via a hot-pressing strategy, J. Mater. Chem. C 7 (39) (2019) 12127–12138.
[61] F. Li, R. Si, T. Li, C. Wang, J. Zhai, High energy storage performance and fast discharging speed in dense $0.7Bi_{0.5}K_{0.5}TiO_3$-$0.3SrTiO_3$ ceramics via a novel rolling technology, Ceram. Int. 46 (5) (2020) 6995–6998.
[62] M. Shiga, M. Hagiwara, S. Fujihara, $Bi_{1/2}K_{1/2})TiO_3$–$SrTiO_3$ solid-solution ceramics for high-temperature capacitor applications, Ceram. Int. 46 (8, Part A) (2020) 10242–10249.
[63] Q. Yang, M. Zhu, Q. Wei, M. Zhang, M. Zheng, Y. Hou, Excellent energy storage performance of $K_{0.5}Bi_{0.5}TiO_3$-based ferroelectric ceramics under low electric field, Chem. Eng. J. 414 (2021), 128769.
[64] L. Chen, F. Long, H. Qi, H. Liu, S. Deng, J. Chen, Outstanding energy storage performance in high-hardness $(Bi_{0.5}K_{0.5})TiO_3$-based lead-free relaxors via multi-scale synergistic design, Adv. Funct. Mater. 32 (9) (2022) 2110478.
[65] X. Dong, X. Li, X. Chen, Z. Tan, J. Wu, J. Zhu, H. Zhou, (1-x)[0.90NN-0.10Bi$(Mg_{2/3}Nb_{1/3})O_3$]-x$(Bi_{0.5}Na_{0.5})_{0.7}Sr_{0.3}TiO_3$ ceramics with core–shell structures: a pathway for simultaneously achieving high polarization and breakdown strength, Nano Energy 101 (2022), 107577.
[66] W. Huang, Y. Chen, X. Li, G. Wang, J. Xia, X. Dong, Superior energy storage performances achieved in (Ba, Sr)TiO_3-based bulk ceramics through composition design and Core-shell structure engineering, Chem. Eng. J. 444 (2022), 135523.
[67] M. Otoničar, S.D. Škapin, B. Jančar, R. Ubic, D. Suvorov, Analysis of the phase transition and the domain structure in $K_{0.5}Bi_{0.5}TiO_3$ perovskite ceramics by in situ XRD and TEM, J. Am. Ceram. Soc. 93 (12) (2010) 4168–4173.
[68] J.T.S. Irvine, D.C. Sinclair, A.R. West, Electroceramics: characterization by impedance spectroscopy, Adv. Mater. 2 (3) (1990) 132–138.
[69] Y. Xie, W. Jiang, T. Fu, J. Liu, Z. Zhang, S. Wang, Achieving high energy density and low loss in PVDF/BST nanodielectrics with enhanced structural homogeneity, ACS Appl. Mater. Interfaces 10 (34) (2018) 29038–29047.
[70] G. Liu, Y. Li, M. Shi, L. Yu, P. Chen, K. Yu, Y. Yan, L. Jin, D. Wang, J. Gao, An investigation of the dielectric energy storage performance of $Bi(Mg_{2/3}Nb_{1/3})O_3$-modifed $BaTiO_3$ Pb-free bulk ceramics with improved temperature/frequency stability, Ceram. Int. 45 (15) (2019) 19189–19196.
[71] F. Yang, Y. Bao, W. Huang, X. Li, Y. Chen, G. Wang, Enhanced energy storage properties of hafnium-modified $(0.7Ba_{0.55}Sr_{0.45}$-$0.3Bi_{0.5}Na_{0.5})TiO_3$-based relaxor ferroelectric ceramics via regulating polarization nonlinearity and bandgap, J. Mater. Chem. C 10 (19) (2022) 7614–7625.